



**University of
Zurich** ^{UZH}

Department of Geography

Quantifying Grassland Degradation in the Borana Zone (Ethiopia)

GEO 511 Master's Thesis

Author

Bernhard Sassik

16-707-093

Supervised by

Dr. Hendrik Wulf

Dr. Rogier De Jong

Faculty representative

Prof. Dr. Michael Schaepman

25.01.2018

Department of Geography, University of Zurich

Abstract

Grassland degradation is defined by loss of productivity and spatial extent. In the Borana Zone, southern Ethiopia, this process threatens the traditional nomadic pastoral culture. Recurrent droughts, increasing population and land cultivation, as well as a ban on fire causing bush encroachment are the main drivers in this process, strongly influencing the regional livestock production and therefore household incomes. Using remote sensing time series, it is possible to identify land cover changes over time and map degraded areas. Likewise, remotely sensed precipitation time series provide information about drought periods affecting grassland productivity.

This master thesis provides insights into local trends regarding the spatial extent and productivity of grasslands by using the Google Earth Engine JavaScript API for the application of a supervised thresholded minimum distance classifier on annually aggregated images of Landsat 5, 7 and 8 that were transformed to useful descriptors based on the Normalized Difference Vegetation Index (NDVI).

Areal grassland loss is mainly introduced by two different drivers: humans and droughts. By regressing per-pixel NDVI sums on sums of precipitation, the respective residuals can be regressed on time to conduct trend analyses and differentiate drivers of degradation. Using this so-called RESTREND method, classification results were linked to overall greening or browning processes that align to the findings in other relevant studies.

Natural grassland disappeared in the north predominantly due to degradation processes, while higher sums of precipitation in the south led to conversions to managed pastures. A flipped rain season in the year 2011 started a short period of general greening which ended by 2013. The combination of annual results and overall trends further revealed effects of multiple consecutive processes over the time series.

Acknowledgments

I want to thank my parents, who made my studies possible and provided me with advice and support!

Thanks to my friends for their support!

Many thanks also to Dr. Hendrik Wulf and Dr. Rogier De Jong for supervising this thesis!

Contents

1	Introduction	7
2	Test Site and Materials	9
2.1	Landsat Data	11
2.2	TRMM Multi-Satellite Precipitation Analysis (TMPA) Data	11
2.3	Training Data	11
3	Methods	12
3.1	Data Preparation and Descriptors	12
3.1.1	Normalizing	12
3.1.2	Moving Window - Slicing	13
3.1.3	Annual NDVI Sum Modeling	14
3.1.4	Pixel Neighborhoods	15
3.2	Clustering and Training Data Collection	17
3.3	Classification and Validation	17
3.4	Residual Trends	18
3.5	Application	19
4	Results	20
4.1	Cluster	20
4.2	Kalos	20
4.3	Natural Grassland	24
5	Discussion	28
5.1	Example: Land Cultivation and Degradation	29
5.2	Example: Early Natural Grasslands to Kalos	30
5.3	Example: Bush Encroachment	30
5.4	Example: New Natural Grasslands to Kalos	31
5.5	Example: Fire Clearing	32
6	Conclusion	33
	References	34

List of Illustrations

Figures

2.1	Maps of the Study Site	9
2.2	Precipitation and Cloud Cover	10
3.1	Available Images per Year	13
3.2	NDVI Slicing	14
3.3	NDVI Sum Modeling	16
3.4	Mahalanobis Distance	17
3.5	RESTREND RMSE	18
4.1	Image Clustering	20
4.2	Kalos: Ground Truth	21
4.3	Kalos: Resulting Charts	22
4.4	Kalos: Resulting Map	23
4.5	Natural Grassland: Ground Truth	24
4.6	Natural Grassland: Resulting Charts	26
4.7	Natural Grassland: Resulting Map	27
5.1	Example: Land Cultivation and Degradation	30
5.2	Example: Early Natural Grasslands to Kalos	30
5.3	Example: Bush Encroachment	31
5.4	Example: New Natural Grasslands to Kalos	31
5.5	Example: Fire Clearing	32

Tables

3.1	Workflow for Descriptor Derivation	15
3.2	Covariance Matrix of Descriptors	15
3.3	Confusion Matrix of P-Classifiers	18
5.1	Reasons for Loss and Gain	29

1. Introduction

The Borana Zone, named after an Oromo clan, is confronted with a great reduction of productive pastures in the last decades [1]. Anthropogenic and naturally induced factors, like bush encroachment due to an official ban of fire in the 1970's and recurrent droughts have severe impacts on local households and their livestock. Herds shrink, leading to decreasing household incomes and increasing poverty as well as food insecurity. Between 1983 and 2003, the average cattle holding per household declined by 54 %, the droughts of 1983/84, 1992/93 and 1999/2000 resulted in a 49 % loss of cattle herd [3]. Such scenarios are mostly followed by declining cattle birth rates, a shortage of milk and slow herd recovery. Pastoralism, the use of natural resources to feed livestock, forces herders to travel long distances between pastures for their cattle and market-centers for trading, making survival based on mobility [19]. However, this extensive form of livestock production gives herders a chance to cope with regional drought events, where crop cultivation fails [3]. In 2009, more common and severe droughts further degraded already heavily used grasslands and water holes, leading to violent conflicts and a drastically reduced mobility due to fear and insecurity [19]. This not only effected herds and their access to pastures, but also herders and their ability to sell their goods on markets.

With help of satellite imagery and remote sensing, it is possible to map and monitor land use and land cover changes to strengthen resilience and coping abilities of communities in such times of distress, as well as suggest or evaluate policies concerning those changes. Also, information from local farmers and their awareness of land degradation are vital for understanding the dynamics of land cover changes. The majority is aware of the increasing problem of grazing land deterioration over the last 40 years, even if it is perceived not as severe in lowlands as in highlands [5]. At the end of dry season, common used grasslands are closed by the elected elders to allow a sufficient regrowth. During this time, watchman enforce this policy of protection.

Several studies over the last ten years focused on the Borana Zone, its land degradation dynamics [1][16] due to droughts [3] and farmers perceptions of this processes [5][18][4][17]. Remote sensing approaches similar to the methods in this study at hand where used in [1], where the authors used unsupervised clustering to identify training regions for a supervised maximum likelihood classifier of seven classes in Yabelo (5426 km²), one of eight Borana districts. Their results were validated with 450 ground truth points and resulted in accuracies between 81.3 % and 84.6 %, depending on different assessed years. [16] clustered eight types of land cover for five different areas within the Borana Zone with a total study area of 735.90 km². They also validated through fieldwork, but with unknown accuracy. For their different test sites, both studies resulted a grassland coverage of roughly 35.5 % to 40 % with a low decrease or even very steep increase of areal extent between 1985 and 2011 (Soda Kebele: +27 % [16]). They connected this increment to an enormous decline in bushland due to successful efforts to reintroduce fire clearings, improved management, grassland enclosures and cessation of grazing.

There is agreement on multiple reasons for grassland degradation in the Borana Zone: bush encroachment [1], conversion to agricultural land, increased numbers of cattle and human population [5], droughts and related shortage of feed and water [17].

The reason for an official ban on fire in the early 1970's was linked to a loss of forest cover in the Ethiopian highlands but lead to bush encroachment [4]. In response to more and denser shrub lands, pastoralists learned to herd camels in addition to cattle [1].

It sounds surprising that droughts and their severe impacts on households lead to crop cultivation, which is more prone to fail due to such conditions, but the participation of pastoral households in agriculture is generally accepted as a way of livelihood diversification in response to economic stress [18]. Though it is highly erratic (successful harvests occur roughly every three years [4]) and yields vary due to precipitation and soil fertility, grain prices are increasing during droughts,

while animal's values decrease. Herders are often forced to sell their livestock at a loss before they die, leaving them with an insufficient herd size to meet their demands. Crop cultivation is a way to substitute this decline, but also creates conflicts by fragmenting and restricting access to prime grazing lands [18]. It is estimated that less than 15 % of Borana households is relying on livestock alone, while the majority relies also on some kind of grains.

The remote sensing community introduced a palette of different methods and approaches to quantify land use and land cover changes, using the optical spectrum of light as well as microwaves [2]. For classification of land quality, unsupervised and supervised algorithms are available. Cluster methods like k-Means group pixels purely based on their appearance descriptors, making prior knowledge (training data) unnecessary. This helps in lack of any information about the study site, but post-interpretation demands for identification of results. Supervised classifiers, on the other hand, enable scientists to input their prior-expertise in form of training datasets. The output will group pixels that are similar to regions that were already labeled as some kind of land cover. Besides, there exist multiple varieties that concern input descriptors, spatial connections or data transformations. Vegetation parameters can further be used in regression models to estimate different dependent or independent variables, respectively. For example can yields be estimated by utilizing the NDVI as performance proxy.

The main goal of this work is the identification of grassland in the whole Borana Zone. This is achieved by applying a supervised thresholded minimum distance classification. The result allows for the quantification of areal extents in a time series of sixteen years. Precipitation data was used for linear regressions, executing the so-called RESTREND method (REsidual TREND) [20]. Its purpose is the identification of vegetation performance trends under consideration of water availability. Since the same methods could be applied to all kinds of land cover classes, an application was developed using the Google Earth Engine Javascript API [9]. It allows the classification and mapping of a variety of classes, purely based on the input training data.

2. Test Site and Materials

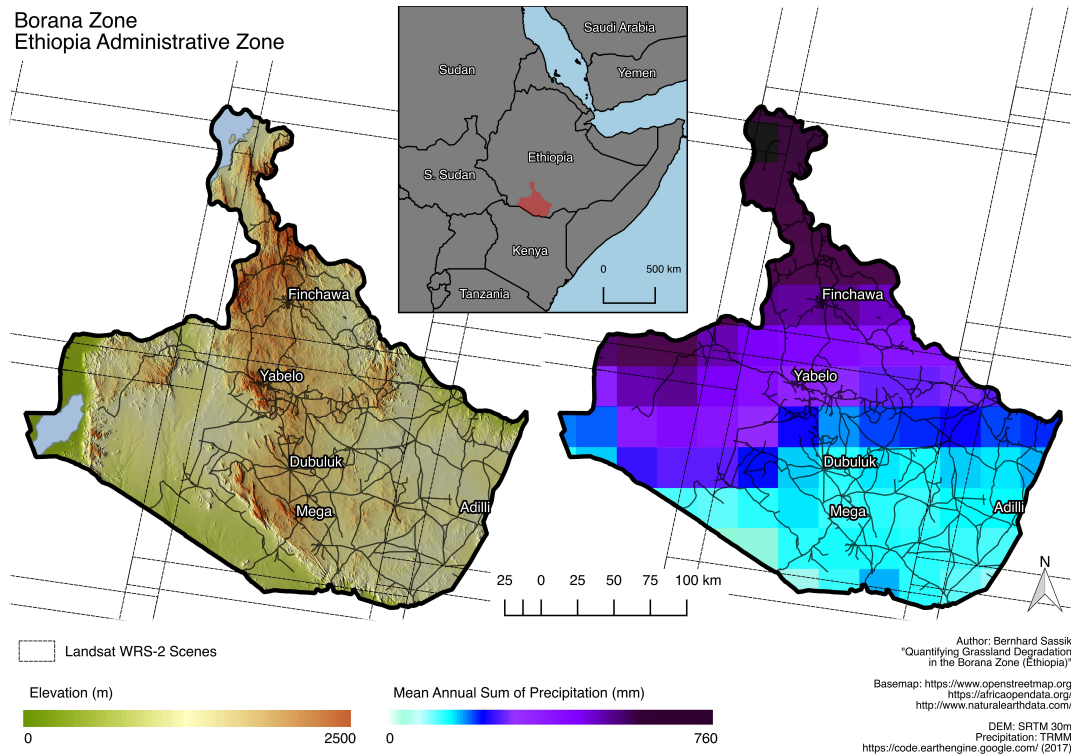


Figure 2.1: Thematic maps of the study area overlaid by Landsat WRS-2 scene boundaries.

The study site is located at 5.05° North 38.20° East and has a total area of 52671 km^2 [Fig.2.1]. Altitudes vary between 450 m in the western flatlands and up to 2487 m (west of Mega) in the highland ridges cutting the area north to south. Besides the slopes of those highlands, the surface is mainly a rather flat plateau at around 1000 to 1500 m altitude. The climate is semi-arid / arid, precipitation occurs primarily in two rain seasons. Roughly two thirds of the annual rain falls around April and one third between October and November [Fig.2.2]. The average annual temperature varies from 19° C to 26° C , with droughts typically every five to six years [1].

Multiple trends are altering the land cover in the Borana Zone. Recurrent droughts degrade grassland and pastures. Cattle herds shrink and households try to compensate the resulting lack of calories with agriculture. A ban on fire led to bush encroachment and regions that reintroduced fire clearings often observed a decline of efficiency, because fire can not spread over degraded bare soil between inflammable bushes. Regional cooperatives introduced so-called *Kalos*, intensively managed pastures around villages, in an attempt to counteract processes of degradation and herd shrinking. Its main concept is to bring all cattle to one *Kalos* after another, providing sufficient time for remaining other pastures to regrow.

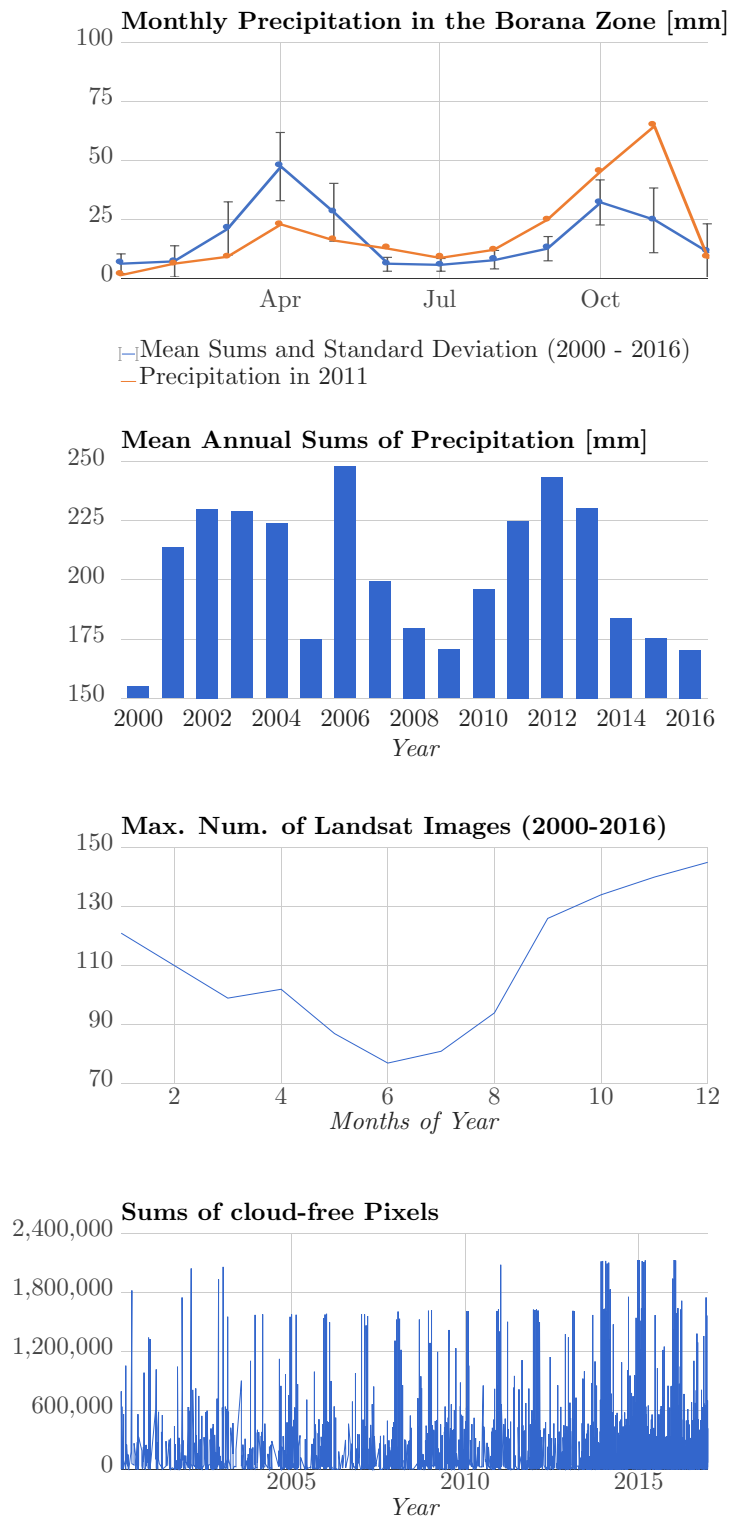


Figure 2.2: The combination of precipitation as a proxy for cloud cover and numbers of taken images per month results in sums of available cloud free pixels. The months December to March have peaks well beyond 1.2×10^6 cloud free pixels, while the value is roughly half around September. Due to the images provided by Landsat 8 starting in 2013, the number of cloud free pixels increased noticeably. The mean annual sums of precipitation reveal droughts roughly every five years.

2.1 Landsat Data

A total number of 2767 Landsat 5,7 and 8 images were used to generate a time series from January 2000 to December 2016. Landsat 5 imagery was available up until 2011, whereas Landsat 8 data could be obtained as of 2013. Per year, this results in approximately 100 to 150 different scenes, respectively 350 in 2013 and after. All images available on the Google servers were atmospherically corrected to surface reflectance and included a cloud mask (using the CFMask algorithm [8]). For dataset merging, Landsat 8 bands were renamed to correspond to the respective wavelengths of Landsat 5/7 bands.

Despite this high amount of imagery, an intra-annual variability in terms of dates of observation needed to be considered for the numbers of images and cloud-free pixels. During rain periods, surface information tends to be hidden by cloud cover. A summation of cloud free pixels resulted in an asymmetric bimodal distribution with highest peaks between the months December to March and less pronounced gradients in September. The reasons for this distribution not only lie within the respective cloud cover, but the fact that there simply were less datasets available, especially over dry seasons, around June [Fig.2.2].

The number of available and used images gets further put into perspective, considering the study site's extent over several Landsat scenes [Fig.2.1].

2.2 TRMM Multi-Satellite Precipitation Analysis (TMPA) Data

The Tropical Rainfall Measuring Mission (TRMM) satellite was launched in 1997 and re-entered the atmosphere in 2015 [12]. The multi-satellite Algorithm 3B42 merges passive microwave data of sensors on multiple satellites (TRMM, DMSP, Aqua, NOAA) and infrared data collected by the international constellation of geosynchronous earth orbit (GEO) satellites to precipitation data in millimeter at a 3-hour temporal and a 0.25° spatial resolution [13][11]. 3B42 continued to exist up until July 2017, while the transition to a new generation, the Global Precipitation Measurement (GPM) and the Integrated Multi-Satellite Retrievals for GPM (IMERG) begun [12].

The TMPA dataset was used to conduct analyses concerning the general pattern of rain and drought in the test area and to link the availability of surface information to cloud cover [Chap.2.1]. Mainly, however, this precipitation data of adequate spatial resolution were used as regressors for aggregated NDVI values in a linear regression model, in order to build trends out of the respective residuals. This residual trend (RESTREND) method enables general statements concerning tendencies of phenological greening or browning processes.

2.3 Training Data

Classification is highly dependent on good training data and necessarily needs to be validated. In this study, areas of grassland and pastures were manually collected with very high resolution imagery of different dates in Google Earth Pro and the support of a clustered image [Chap.3.2]. The training polygons were sampled to points on a 30 x 30 meter grid. Based on their descriptor values, a class centroid was built in their mean as an ideal representation of considered land cover type.

3. Methods

To tackle research questions concerning grassland, a first obvious step is to classify this specific land cover type. Since no a priori information was considered, an unsupervised k-Means clustering was executed to group pixels to distinctive classes, based on their respective descriptors. The cluster manually identified as grassland helped to train a classifier by pointing out regions to collect sufficient training data from. The minimum distance classifier built with these selected grassland regions was thresholded and verified with the training set and a separated validation set. By applying the trained classifier on image compositions of every year in the series, a changing spatial extent of grassland was documented.

In an initially independent approach, annual sums of NDVI per pixel were modeled and used as dependent variables in a linear regression model with annual sums of precipitation per pixel. As these NDVI sums turned out to be valuable and informative pixel descriptors, they were further considered in the classification. Assuming that rain is the main influencer of vegetation's ability to grow in arid or semi-arid areas, the residuals of these regressions provide information about greening or browning tendencies under consideration of water availability. Further, they can themselves be regressed over time to calculate slopes of trends.

The NDVI forms the normalized difference of infrared and red reflectance to an index that is strongly correlated with vegetation productivity [7]. It has a theoretical value space of [-1,1] but interpretable results vary between 0 (no photosynthesis) and 1 (very high productivity). Trends of this value can be used as a proxy for photosynthetic activity changes [6].

3.1 Data Preparation and Descriptors

The right set of pixel descriptors has high impact on successful classification efforts. To some extent, a choice on these variables also determines the temporal resolution of the result. A basic criterion that needs to be met in such a consideration, is that every pixel is represented in every time step, setting the minimal temporal resolution to an interval that can fulfill this demand. For the test site, temporal units shorter than a calendar year, for example rain or phenological seasons, could not meet this requirement [Fig.3.1]. By aggregating the data to annual bins and therefore over whole growing cycles, risks of effects of the Modifiable Temporal Unit Problem (MTUP), describing influences of aggregation levels and starting phases on respective model results, were minimized [6].

The following subsections explain the different methods used to extract certain descriptors. A bold line at the end of each subsection summarizes the respective inputs and outputs.

3.1.1 Normalizing

All bands were used in the surface reflectance value space. The descriptors for the classifier, which includes the Landsat bands itself, needed to be in similar dimensions, since distance measurements in the classification process are related to the respective descriptor variances. A distance of 1 would for example include the complete interpretable value space of NDVI, while excluding all observed Landsat band values, scattering around ± 10000 . Since an ordinary value normalization $(x_i - \min(x)) / (\max(x) - \min(x))$ resulted in computational timeouts and insufficient execution speed, all Landsat bands were simply divided by 300 to resemble to annual NDVI sums spreading between 5 and 15, even though this step does not influence intra-annual intra-regional data variabilities over multiple Landsat scenes and therefore is not a real normalization in a strict sense. To further overcome the problem of a need for similar dimensionality, distance measurements in

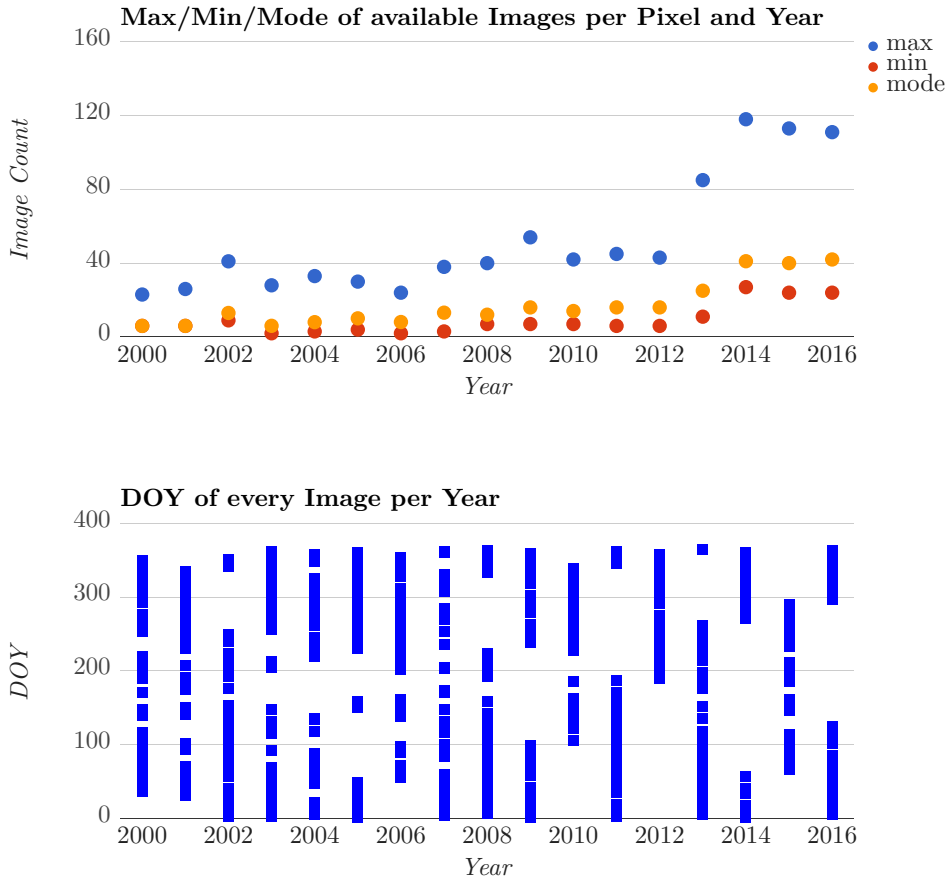


Figure 3.1: An aggregation to annual values per band ensured that every pixel was considered in every step. The temporal distribution of observations did not follow any particular pattern, but shows intra-annual gaps and tends to a year's shoulder.

the classification algorithm were based on mahalanobis distances rather than euclidean differences, which take respective variances into account [Chap.3.3].

B[1-7] → Normalizing → Mean of Bands in dimensions of roughly [0,15]

3.1.2 Moving Window - Slicing

365 days were in the most extreme cases represented by just six observations, also including those that are actually clouded, scattered over the year without any particular pattern [Fig.2.2][Fig.3.1]. An empirical analysis of random sample pixels showed errors for the preprocessed cloud masks in form of outlying very low or negative NDVI values in the respective pixel's time series. On the other hand, very high NDVI values which can be seen in relation to their dates of respective observation were found. If an image is available on a Day Of Year (DOY) where the growing cycle happens to peak, the time series consequently includes a relatively high valued record, but a pixel of the exact same land cover class lacking just this particular observation will show a lower average as a result. Therefore, whole observations represented by the top and bottom 30 % NDVI values per pixel were sliced in a window of three years [Fig.3.2]. Specifically, a pixel's NDVI values for the respective years y_{-1}, y, y_{+1} were sorted in an ascending array to pick the maximum of the bottom and minimum of the top scoring 30 %. In the following masking process, only observations higher than the maximum low-value and lower than the minimum high-value are allowed to be reduced to band mean values per year. For this procedure, the NDVI must be considered a quality criterium in such, that a whole observation with all its respective bands and represented by its

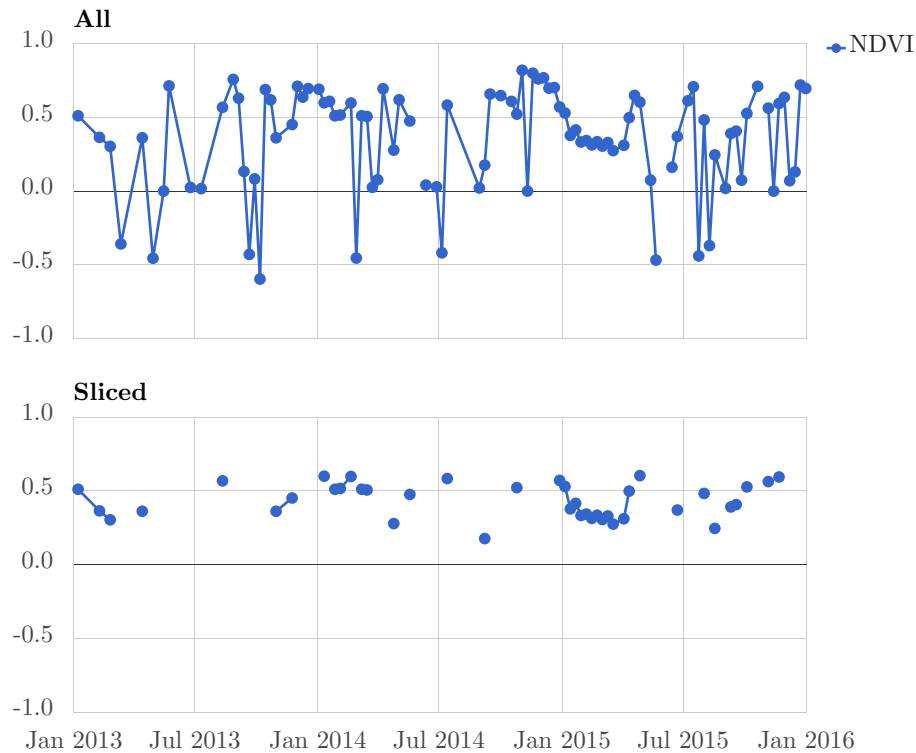


Figure 3.2: A visual example of the masking process of extreme values for the year 2014 at a random point. By slicing outliers, the average of remaining bands changes. The sliced observations are assumed to better represent a class in the whole time series by eliminating extremes introduced by observation circumstances.

NDVI, can potentially be masked. Slicing 60 % of observations in total leaves less than half the sample size with mediocre values to average but also eliminates outliers introduced by observation circumstances. Since the modeled sum of NDVI resulted in more homogeneous results, the sliced NDVI mean itself was not used as descriptor, but only the 3-year-means of the remaining not sliced Landsat bands [Chap.3.1.3]. In order to account for Landsat 7 Scan Line Errors these band means were further averaged to local means in a 500 m radius in one iteration [15].

B4,B3 → **NDVI** → **Slicing** → **Local means** → **3-year-mean of bands**

3.1.3 Annual NDVI Sum Modeling

All assumable cloud free NDVI values > 0 , including also sliced observations, were considered in a linear regression model that reduces a pixel's values per year to multiple sine waves. A single such wave can be written as a linear combination of $a * \sin(x) + b * \cos(x)$, where x is set based on the desired frequency [10]. By linearly combining waves of different frequencies, non-harmonic waves can be modeled. Multiple sine waves with wavelengths $\lambda = year/[2, 4, 6, 8]$ were considered to model sums of NDVI, primarily for the RESTREND analysis, but also as classification descriptors.

A regression model of eight independent variables (four waves with two coefficients each) but, in the worst case, only six dependent ones (real NDVI observations), inevitably fails due to under-determination. Hence, annual sums of NDVI were obtained by merging all observations in the time series 2000 - 2016 to a single artificial year, based on their respective DOYs. The resulting regression model of waves in different lengths forms a general shape of signal evolution for a modeled year. Every pixel's individual general shape was again modified for the different years by concatenating modeled NDVIs for every tenth DOY and replacing values where real observation of respective year are available. The resulting array was again regressed over four different sine waves, with real values weighted by a factor 50 in the underlying residual optimization of regressions [Fig.3.3].

The respective NDVI sums were masked to $0 > NDVI > 40 = 0$ in order to reduce meaningless variance produced exclusively by water surfaces.

NDVIs in whole time series → Sine wave modeling → Annual sums of NDVI

3.1.4 Pixel Neighborhoods

Every pixel’s descriptor space was widened by including the mean of its directly neighboring pixel’s annual sums of NDVI. Doing so, the probability for a pixel to be classified as a specified land cover type increases if it’s surrounding neighbors also look similar to the class in terms of NDVI sums. To prevent errors due to the neighbor’s sequence of appearance in the descriptor matrix, the values were reduced to a single mean.

Sum of NDVI → Mean for eight neighbors

In summary, the data set was heavily modified in the preparation phase. In extreme cases and with exception of the slicing procedure, six different observations per pixel and respective year were transformed to following descriptors [Tab.3.1]:

- 3-year-mean of sliced Landsat Bands [1-7], averaged over a 500 meter kernel
- Modeled NDVI sum
- Mean of eight neighboring pixel’s NDVI sums

Table 3.1: Simplified workflow of the Landsat 5, 7 and 8 data aggregation for the derivation of descriptors.

<i>Landsat 8 Bands</i>	B2	B3	B4	B5	B6	B7
<i>Landsat 5/7 Bands</i>	Rename to ...					
<i>Spectrum</i>	B1	B2	B3	B4	B5	B7
<i>LS7 Wavelength (μm)</i>	Blue	Green	Red	NIR	SWIR1	SWIR2
<i>Derived Descriptor</i>	0.0441 - 0.514	0.519 - 0.601	0.631 - 0.692	0.772 - 0.898	1.547 - 1.749	2.064 - 2.345
<i>Derived Descriptor</i>	Modeled NDVI sum					
	Mean of neighbors					
	Slicing					
	Normalizing					
<i>Derived Descriptor</i>	Sliced B1 mean	Sliced B2 mean	Sliced B3 mean	Sliced B4 mean	Sliced B5 mean	Sliced B7 mean

The covariance matrix for all descriptors shows their mutual connections [Tab.3.2]. A high variance of a certain variable makes clean thresholding for respective classes easier. Covariance provides information concerning the relationships among descriptors in the respect, that a high covariance is an indicator of the tendency that two variables describe the same fact. That is the case for NDVI sums based on bands 3 and 4, which are mostly similar to their neighbor’s. Bands 5 and 7 have respective maximums resembling to NDVI sums, which results in similar variances.

Table 3.2: Covariance Matrix for the selected descriptors in 2016 in a spatial subset and multiplied by 100 in following order: **1**: Sliced B1 mean, **2**: Sliced B2 mean, **3**: Sliced B3 mean, **4**: Sliced B4 mean, **5**: Sliced B5 mean, **6**: Sliced B7 mean, **7**: Modeled NDVI sum, **8**: Mean NDVI sum of neighbors

	1	2	3	4	5	6	7	8
1	12.399	18.752	30.938	29.573	49.108	48.323	-32.225	-31.625
2	18.752	30.827	56.18	53.01	87.903	87.57	-62.669	-61.283
3	30.938	56.18	124.9	101.648	192.411	202.957	-175.729	-171.767
4	29.573	53.01	101.648	117.631	159.925	149.763	-83.737	-82.798
5	49.108	87.903	192.411	159.925	336.471	348.275	-263.496	-256.824
6	48.323	87.57	202.957	149.763	348.275	385.739	-313.4	-304.83
7	-32.225	-62.669	-175.729	-83.737	-263.496	-313.4	395.621	383.88
8	-31.625	-61.283	-171.767	-82.798	-256.824	-304.83	383.88	377.276

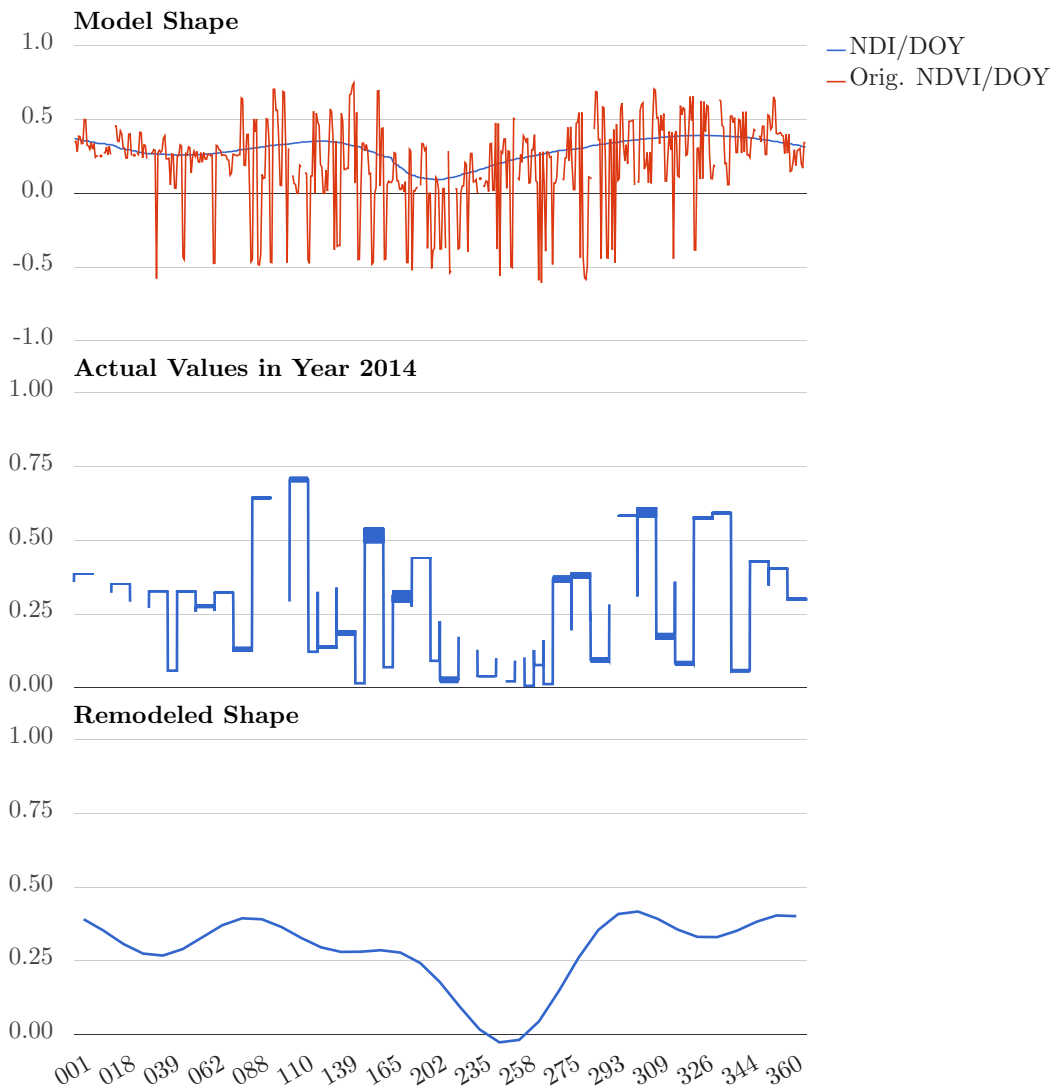


Figure 3.3: Based on all observations ($NDVI > 0$) in the time series, an individual general model shape was calculated for each pixel. By introducing a respective year's real values 50 times each to a further regression model, the general shape was modified. Note that the plateaus for actual values are a result of this weighting, since every real value was introduced to the model with 50 independent observations.

3.2 Clustering and Training Data Collection

An unsupervised k-Means clustering of the aggregated descriptor image for the year 2013 helped to get a first impression of different present land cover classes. Most high resolution images available and used for training data collection were taken between 2012 and 2014, making 2013 a legitimate approximation. The method of clustering is independent from any training data and a priori information, but only groups pixels to k classes based on their respective descriptors and distance/resemblance to each of those groups. Every group has its centroid in a n -dimensional space, where n is the number of descriptors, in the mean of all their belonging pixels. Using k-Means, the number of different groups to distinguish is up to be guessed and approximated by the user. Based on visual interpretation of very high resolution imagery in Google Earth Pro, $k = 10$ was identified as a good fit to render grassland areas in reasonable matters for further manual data collection.

3.3 Classification and Validation

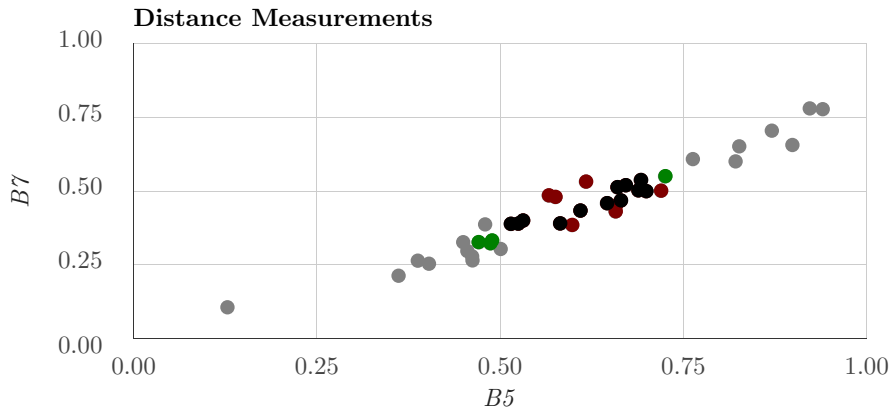


Figure 3.4: In this example, 40 random pixels were visualized and thresholded in the descriptor dimensions B5 and B7 (sliced annual means), as they have high variance and covariance to each other [Fig.3.2]. While some points are included in both distance measurements (black), the euclidean distance (red) thresholds the data points in a circle around their means and the mahalanobis isodistance (green) has an elliptic shape. Descriptors with a lower variance like the mean of B2, thresholded with euclidean isodistances, would potentially yield false-positives.

Without exhaustive training datasets and knowledge of all existing land cover classes, multi-class classifications introduce unnoticeable errors by assigning pixels of unknown or untrained classes to one that the algorithm learned [14]. This can be avoided by performing a one-class classification, where samples are only available for one class of interest. Contrary to using another subcategory, the PU-classifiers (positive and unlabeled training data), this study uses a P-classifier and therefore only positive samples for training. In consequence, just a producer’s accuracy but no confusion matrix or other standard parameters like user’s accuracy and Cohen’s kappa are extractable, since it can not be assumed that all points not included in the training dataset are not part of the class [Tab.3.3].

The chosen classifier is based on mahalanobis distances in the 8-dimensional descriptor space. In a first step, the training dataset consisting of multiple polygons is sampled to points on a 30 x 30 meter grid. 30 % of these samples were separated for later validations. A reference year, which is the year for which it can be assumed that the training is correct, needs to be set based on information about the training data collection process.

The algorithm exclusively uses the training points to build a class centroid in the mean of all their respective descriptors for the reference year. This center is then used for distance measurements to the respective descriptors of every single pixel in the test site for every year in the time

Table 3.3: If only samples of a single class were trained (t_+) for a P-classification, it is not possible to know how many positive (r_+) or negative (r_-) classified results actually are samples of another class (t_-). In consequence, only one producer’s accuracy, which is the probability that the trained land cover is classified as such, is available. Table based on [14].

	t_+	t_-	UA
r_+	✓	x	x
r_-	✓	x	x
PA	✓	x	x

series. To take data variance into account, the mahalanobis distance was deployed. Euclidean isodistance would allow high variations in dimensions with actual low variance, while mahalanobis isodistances enables thresholding of the data preferred along more variable dimensions [Fig.3.4]. The continuous valued output ultimately needs thresholding for conversion in a binary value space.

For this study, thresholding was done manually based on validation results and visual interpretation of respective outputs. The training dataset was narrowed by extracting a separate validation set. An underestimated threshold is indicated by many excluded training and validation points, vice versa for overestimation. Further, overfitting is indicated by included pixels that are not part of the class by means of visual interpretation.

Two tools were made available to set a satisfying threshold. First, the relative numbers of training and validation points considered to be part of the class based on a respective threshold in a moving five-integer-increment interval provide information about how broad or narrow a selected threshold would be under consideration of false-negatives (producer’s accuracy). This chart will further be referenced to as accuracy chart [Chap.4]. Second, a histogram of distance values in the study site helps to put the accuracy chart in perspective in so far, as it indicates the possibility of false-positives using a certain threshold.

3.4 Residual Trends

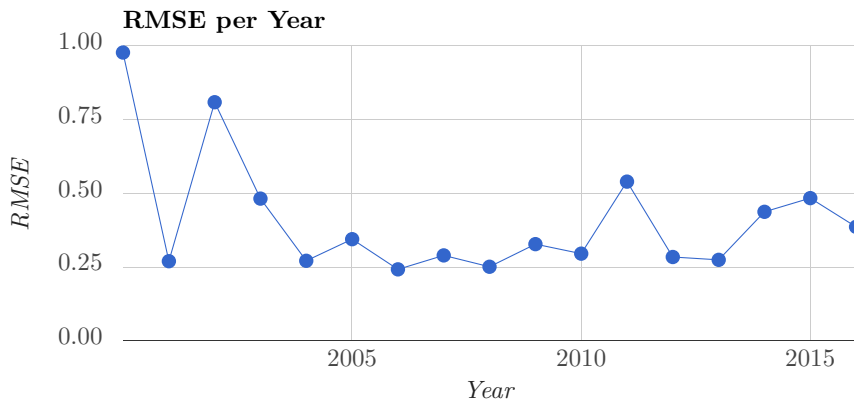


Figure 3.5: The annual root mean square errors of every year’s pixels regression show average model deviations of up to 20 %. The respective errors of each pixel per year got regressed over time to conduct the RESTREND analysis.

In the initial approach, the method is completely independent from any classification efforts. Assuming that the annual sum of precipitation is the main driver and preventer of vegetation growth in arid and semi-arid parts of the world and that the NDVI sum is a satisfying proxy for photosynthetic activity, all pixels in the test site can be reduced to linear regression models of those two variables. Specifically, the natural logarithm of rainfall sums is assumed to be in a linear relationship with sums of NDVI, since vegetation production reaches a plateau in years of very high

precipitation [20]. The models can be oriented in two different dimensions, by either reducing all pixels per year (regional reduction) or all years per pixel (temporal reduction). The total number of reductions depends on a decision in that matter and equals to one model per year or one model per pixel, respectively. The main disadvantage of a regional reduction is an inevitable dependency of the resulting map from the spatial resolution of the independent regression parameters, specifically the lower resolved precipitation data. Every NDVI pixel within a single precipitation pixel is assumed to have the same NDVI, so the calculated residuals show an overall tendency in one direction. On top of this tendency, actual differences in land cover types and their vegetation performances become apparent. These spatial dependencies can be avoided by deploying temporal reductions. Here, every pixel has sixteen tuples of NDVI and precipitation. Based on those, a NDVI value can be modeled per pixel that has a spatial dependency on only itself.

The RMSE, root mean square error of these pixel-based models per year reveal a high dependency of photosynthetic activity from total precipitation. With NDVI sums roughly between 5 and 15, a RMSE of 1 equals to an accuracy of at least 80 % [Fig.3.5]. Also, the respective annual residuals, which are a pixel's deviation from the model, were calculated to quantify the difference between an actual NDVI and the value predicted by the model per year. These residuals indicate greening performance under consideration of water availability. To account for Landsat 7 Scan Line Errors which lead to stripes within the scenes and gain a homogeneous result, the residuals were averaged to a pixel's respective local mean of 500 meters in one iteration [15].

By calculating a pixel's series of residuals over time, another version of linear regression model can be obtained, where those residuals are dependent variables of the independent time constant. The resulting trends can be linked to degradation processes over time.

Other studies also use annual sums of NDVI as estimation of total photosynthetic activity [20]. Due to lacking yearly data for this study, NDVI sums were modeled [Chap.3.1.3]. Doing so, every year was represented by a homogeneous sample and sample size, removing all dependencies between calculated sums and total numbers of available observations.

The Kendall-Tau correlation [-1,1] is a ranked-based non-parametric test of the null-hypothesis that the residuals are ordered randomly over time. A positive tau value indicates an overall increasing trend, a negative value a decreasing, but it tells nothing concerning the severity of trends. In its essence, it is a reduction of sixteen different residuals per pixel to a single representative value that provides a general impression of greening or browning trends.

3.5 Application

The same methods were executed for two land cover classes, natural grasslands and managed pastures, and can potentially be applied to every conceivable trained class. The procedure always follows the same basic steps, so an application was developed for faster and standardized processing. The workflow consists of following steps:

- Collect ground truth (e.g. in Google Earth Pro) and import it as fusion table
- Set appropriate reference year and assess training data set
- Export resulting classification image and a separated set of points for validation
- Convert the validation set to a fusion table and rename column "system:index" manually to any other name
- Import classification image and fusion tables with a set reference year
- Pick of a threshold based on mapped results and the accuracy charts
- Assessment of trends in areal extents and maps for different years
- Assessment of individual pixels
- Assessment of RESTREND results, general and per pixel
- Export of maps as .TIF for further processing

The output of the classification is an image where each pixel contains the distance to the trained class centroid. By defining which distances are still close enough to the centroid, these continuous values get transformed in a binary image mask.

4. Results

Using the developed application, two land cover classes were assessed. *Kalos* ground truth samples were easy to find due to their distinctive shapes. Natural Grassland, on the other hand, was difficult to train because of an ambiguous appearance that often and depending on the observation date either resembled bare soil or indicated overlapping with many trees or bushes.

4.1 Cluster

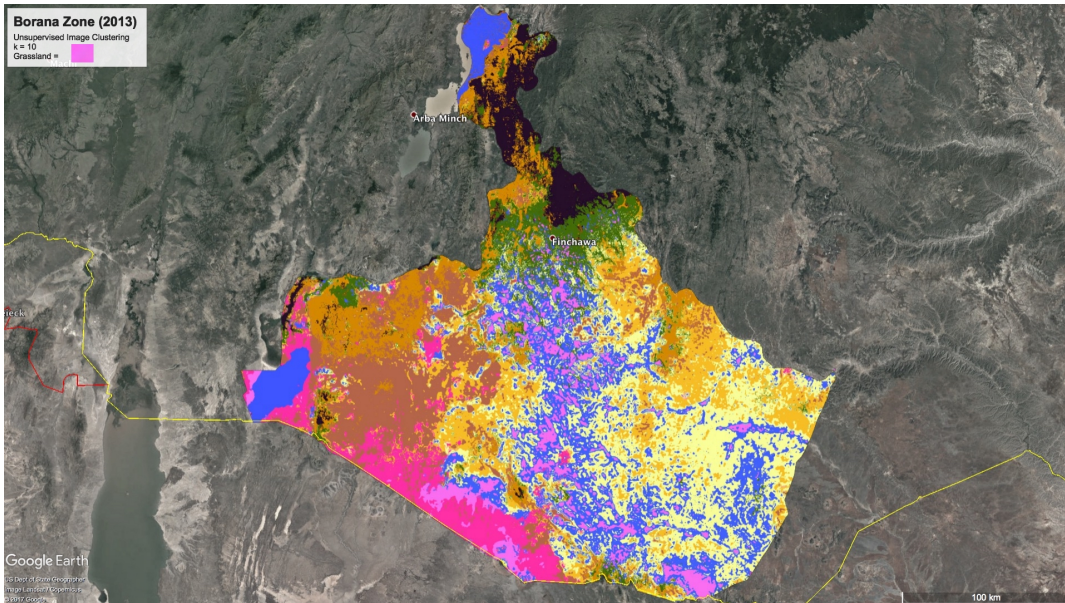


Figure 4.1: The pink cluster was identified as grassland. Training data for both minimum distance classifications was obtained under consideration of this result.

Multiple unsupervised k-Means clusterings were performed and tested, with $k = [3, 16]$. Since the primary goal was not necessarily a homogeneous image segmentation but only the identification of potential grasslands, $k = 10$ was picked as best fit for this land cover type, based on a visual result interpretation [Fig.4.1].

4.2 Kalos

Kalos are intensively managed grazing enclosures for cattle. These pastures are fenced by bushes in mostly geometrical shapes, making them reasonably easy to find [Fig.4.2]. 86 such *Kalos* were located randomly on the test site and sampled to 1713 points. 1192 of them were used for training, 521 were excluded for validation. Google's very high resolution images of the area were mainly from the years 2012 and 2014, making 2013 a legitimate approximated reference year. The distance threshold was set based on accuracy results and visual map interpretation [Fig.4.3]. $t = 4.4$ yielded a classification accuracy of 95.1 % for validation data, which is the relative number of points that

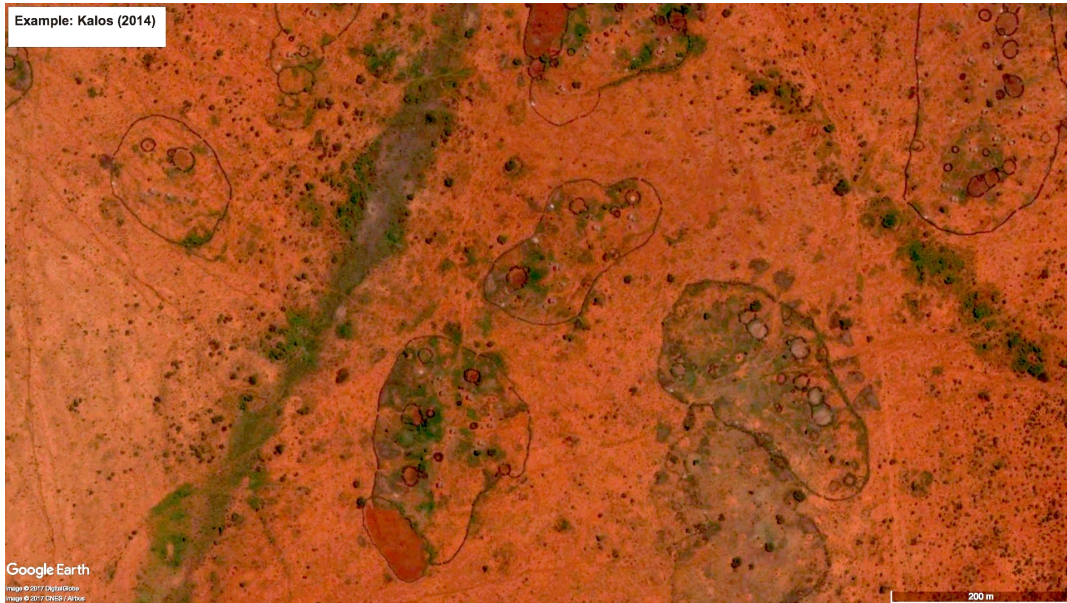


Figure 4.2: Ground truth example for *Kalos* with its distinctive shape. These fenced pastures provide food for cattle of nearby villages.

were actually considered in the resulting class. Higher thresholds could not substantially further increase the accuracy but only made false positives more likely.

The result shows a clear increase of managed pastures between 2011 and 2016 [Fig.4.3]. The areal extent raised by two thirds in 2013 alone and reached over 3500 km² in 2015. Besides the buffer zones around already existing pastures, substantial areal gain was reached as of 2012 in the northern flatlands between Finchawa and Yabelo, where class distances notably decreased for pixels with also generally slightly decreasing RESTREND residuals and therefore negative Kendall tau coefficients [4.4]. In other words, residual trends tend to be inverse proportional to their likelihood of being classified as *Kalos*. Southeast of Yabelo, the Kendall's tau for newly gained areas was notably lower. For a patch southwest of Dubuluk, where land was also gained, this connection inverted in so far, as areas with positive Kendall tau values showed a tendency of decreasing class distances and therefore a higher probability of being pastures.

In general, *Kalos* could be found close by and around settlements or vice versa, people historically settled close to suitable lands. The same is true for most parts of newly gained land of this surface cover type. A majority of pixels newly classified as *Kalos* after 2011 has negative trends of residuals, meaning over the time series they performed worse in terms of photosynthetic activity under consideration of available water, but exactly this performance loss made them more likely to be identified as pastures.

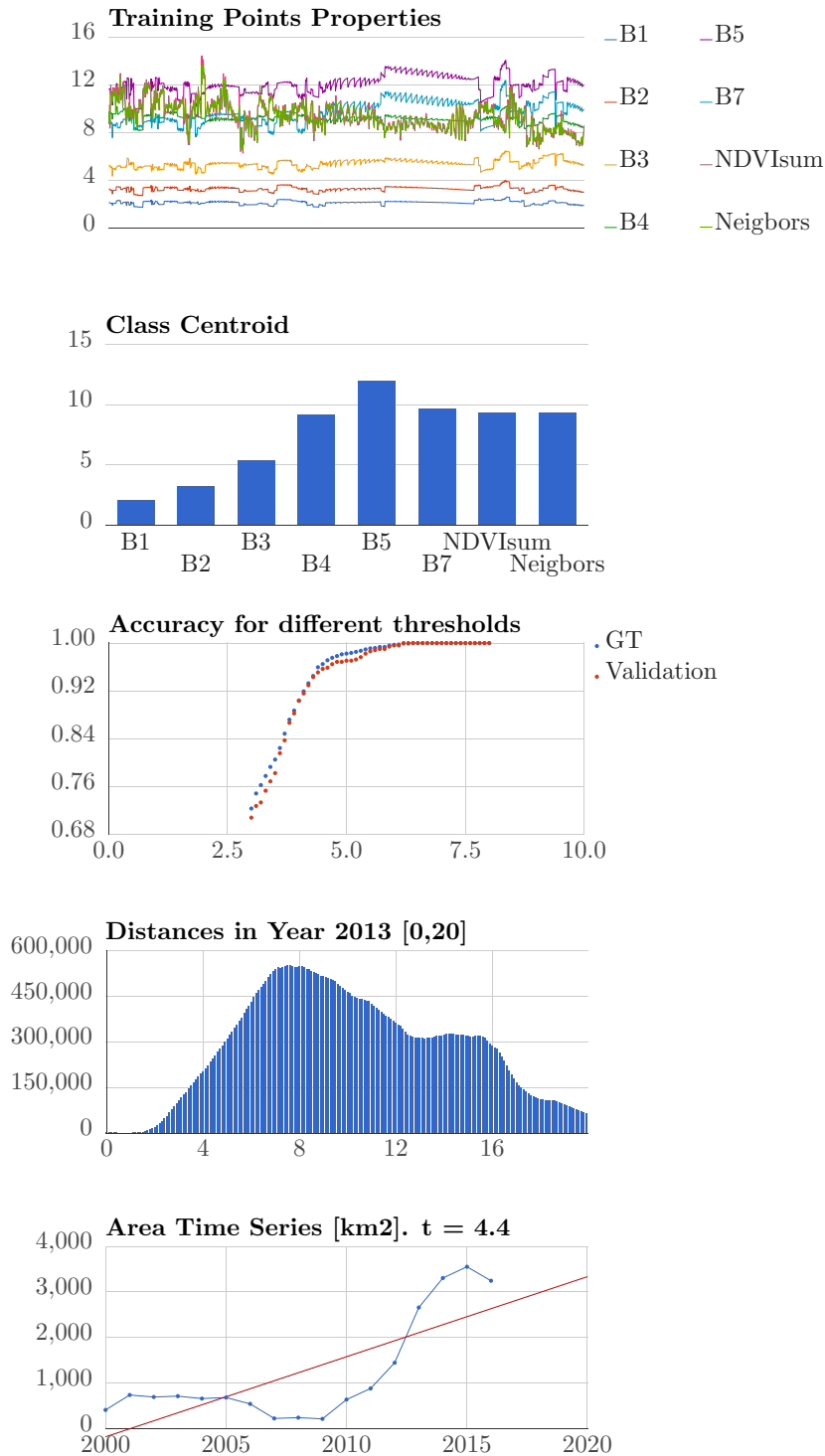


Figure 4.3: Kalos: The descriptor means of all respective training points build the class centroid, an ideal but averaged representation of desired class. The threshold defines a necessary similarity between a pixel and the centroid in order to still be considered part of the class. For $t > 4.4$, increasingly more unlikely pixels are included in the class without the benefit of a satisfying higher accuracy, which means the inclusion of training points into the class.

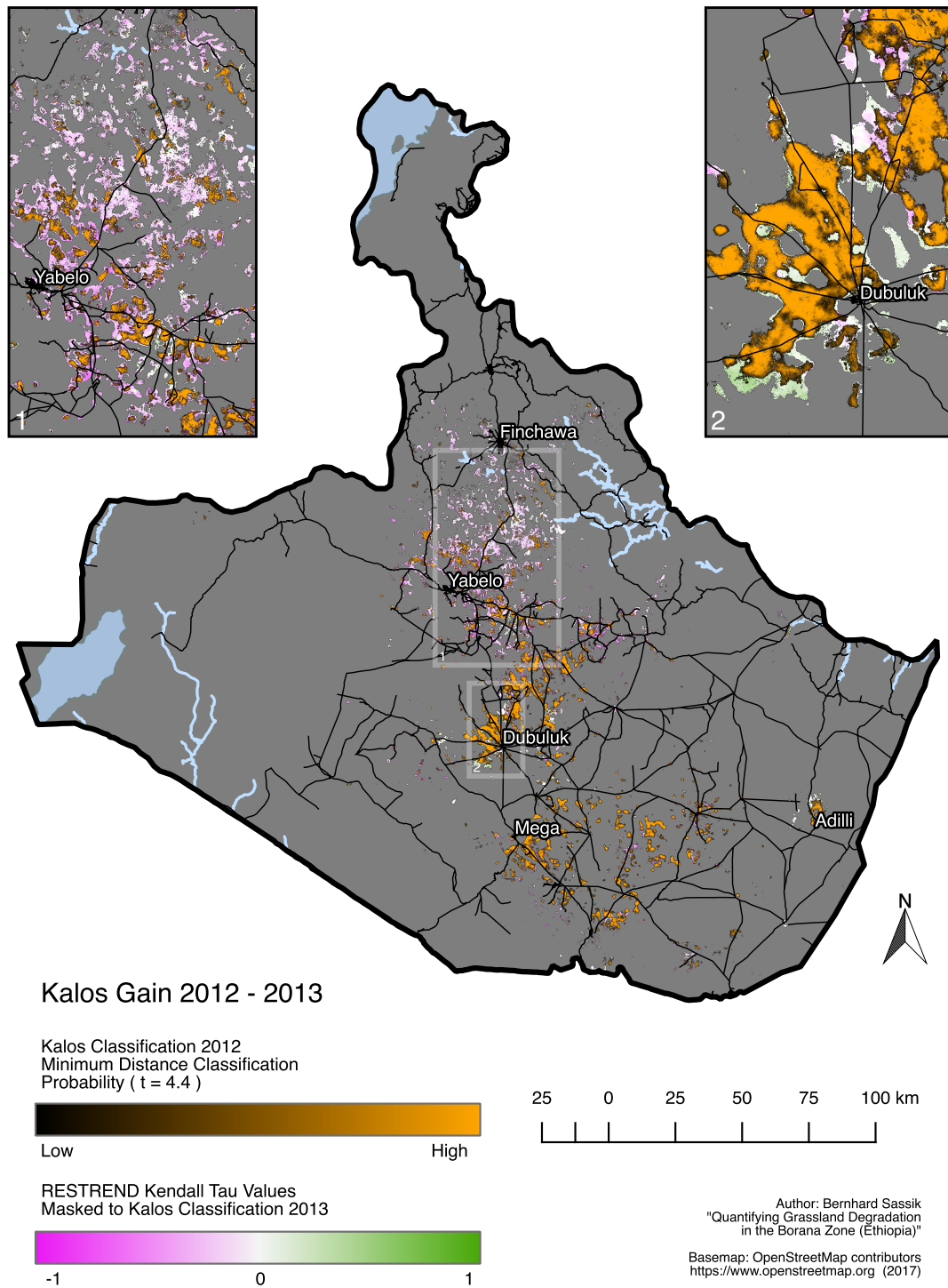


Figure 4.4: *Kalos* as classified in the year 2012. RESTREND Kendall tau values were masked to all pixels classified in 2013 to present areal gain, which can mainly be observed between Finchawa and the central area of Yabelo. In the south, small patches with a positive Kendall's tau around the settlement Dubuluk transformed to *Kalos*.

4.3 Natural Grassland

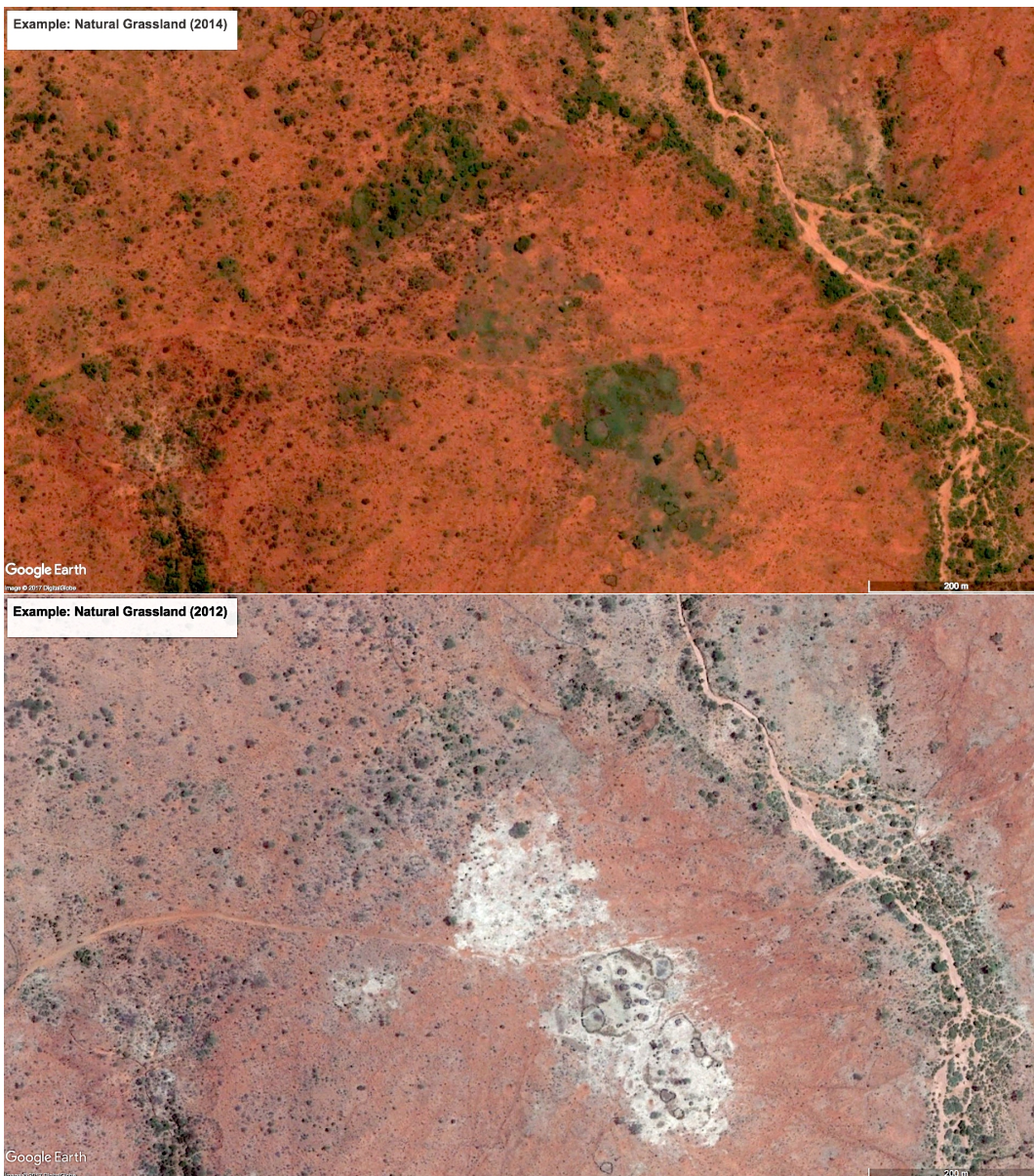


Figure 4.5: Ground truth examples of natural grassland. The appearance in different observations is highly depending on respective prevailing conditions like water availability.

Natural grassland was trained exclusively with very high resolution imagery of dry season 2012. Within the identified grassland cluster, bright white spots were collected, as they were assumed to be natural green grasslands in wet seasons [Fig.4.5]. 36 polygons were sampled to 537 training points and 223 validation samples. Because of ambiguous appearances, many potential training spots were left out, leaving a relatively small dataset to work with. Remaining trained regions were therefore assumed to be pure and made a high accuracy desirable. A steady increase of included training points existed for thresholds ≤ 4.1 , suggesting this very value as widest distance reasonable to pick. 95.4 % of the validation dataset is considered part of the natural grassland class under this consideration [Fig.4.6].

For the first half of the time series, natural grasslands occupied a quite steady total area of roughly 250 km², although regarding result alone does not prove that no shifts and movements

took place in these years. 2011 and 2012 brought a notable increase, in 2011 75 % more pixels were considered grassland than the year prior. In 2013, however, even more than this new areal gain was radically lost again.

While the vast majority of grassland pixels between Finchawa and Yabelo were lost in regions of a negative Kendall's tau, this relation turned for many lost parts in the south [Fig.4.7]. There is a notable correlation between increasing classification distances and also positive RESTREND results for southern grassland areas around Dubuluk and roughly 60 km west of Mega.

In comparison, some areas were classified as both, *Kalos* and natural grassland. The class centroids built with respective training datasets present very similar shapes that were on a just slightly lower overall level for *Kalos*, where especially the modeled sums of NDVI were lower. By widening the variances still acceptable for successful classifications under consideration of certain thresholds, pixels could in consequence appear similar enough to be part of either class. Between Finchawa and Yabelo both classifications cumulate pixels, in some cases the same. These double classifications could be categorized as errors, but in consideration of years mapped differently in [Fig.4.4] and [Fig.4.7], many actually indicate land cover conversions from natural grasslands to managed *Kalos*. As will be discussed, this is also and especially true for the region around Dubuluk, where pixels were mapped in a transition phase [Chap.5].

Both examined land cover classes simultaneously had growing phases initiated around 2011 / 2012. Strikingly, the normal rain pattern flipped in 2011 and brought two thirds of total precipitation in the second rain season around November [Fig.2.2]. The following peak in April 2012 again accounted for two thirds of total precipitation for the year. In other words, two abundant rain seasons occurred within half a year. This was the only such case in the time series and it further amplified the effects of already increased availability of water around the year 2012 [Fig.2.2].

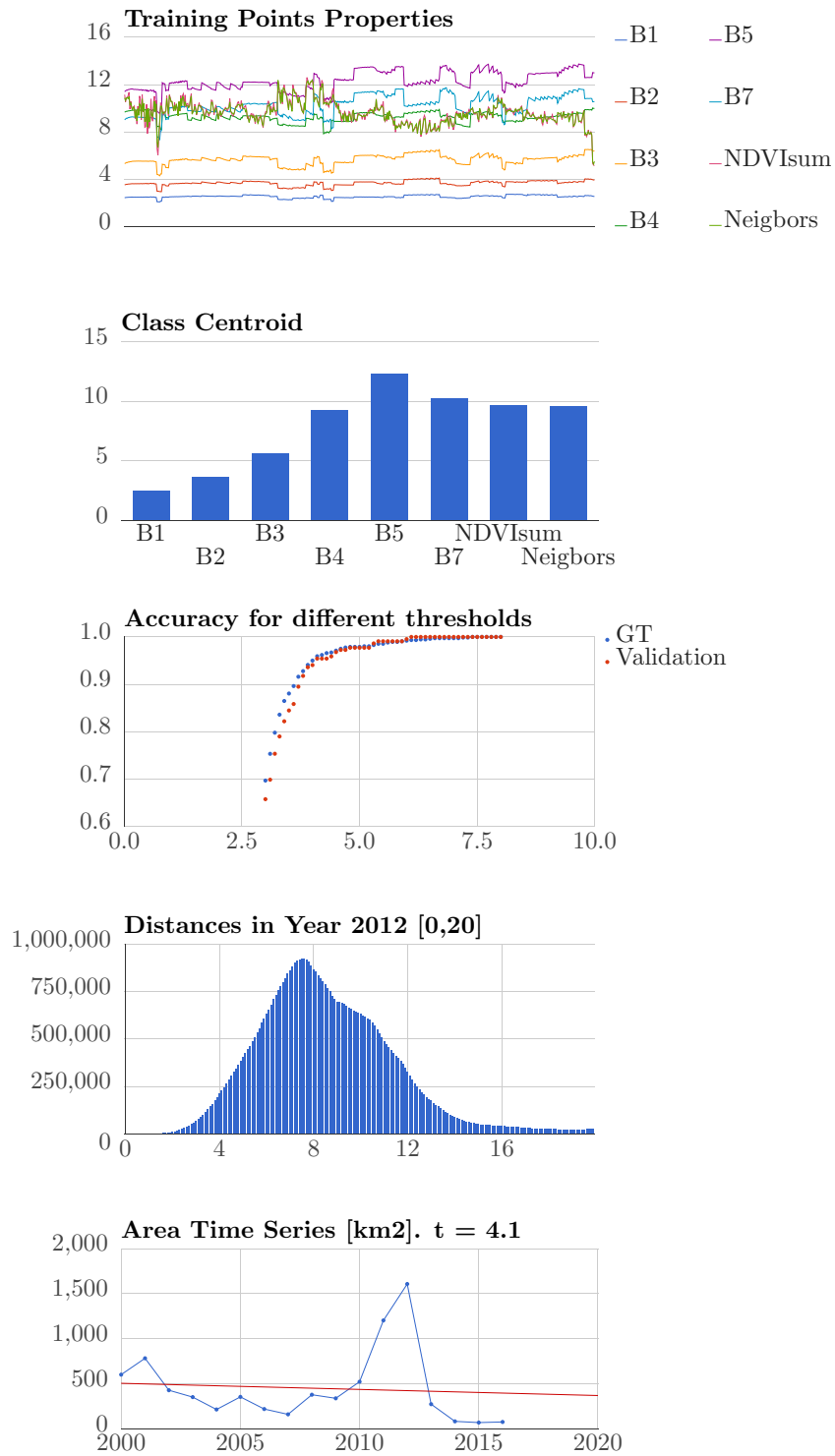


Figure 4.6: Natural grassland: The steady increase of more included training data points stopped for $t > 4.1$. The resulting spatial extents per year show a slightly negative general trend, but a high extremes for the years 2011 and 2012. Also, a following step decrease under previous levels is notable.

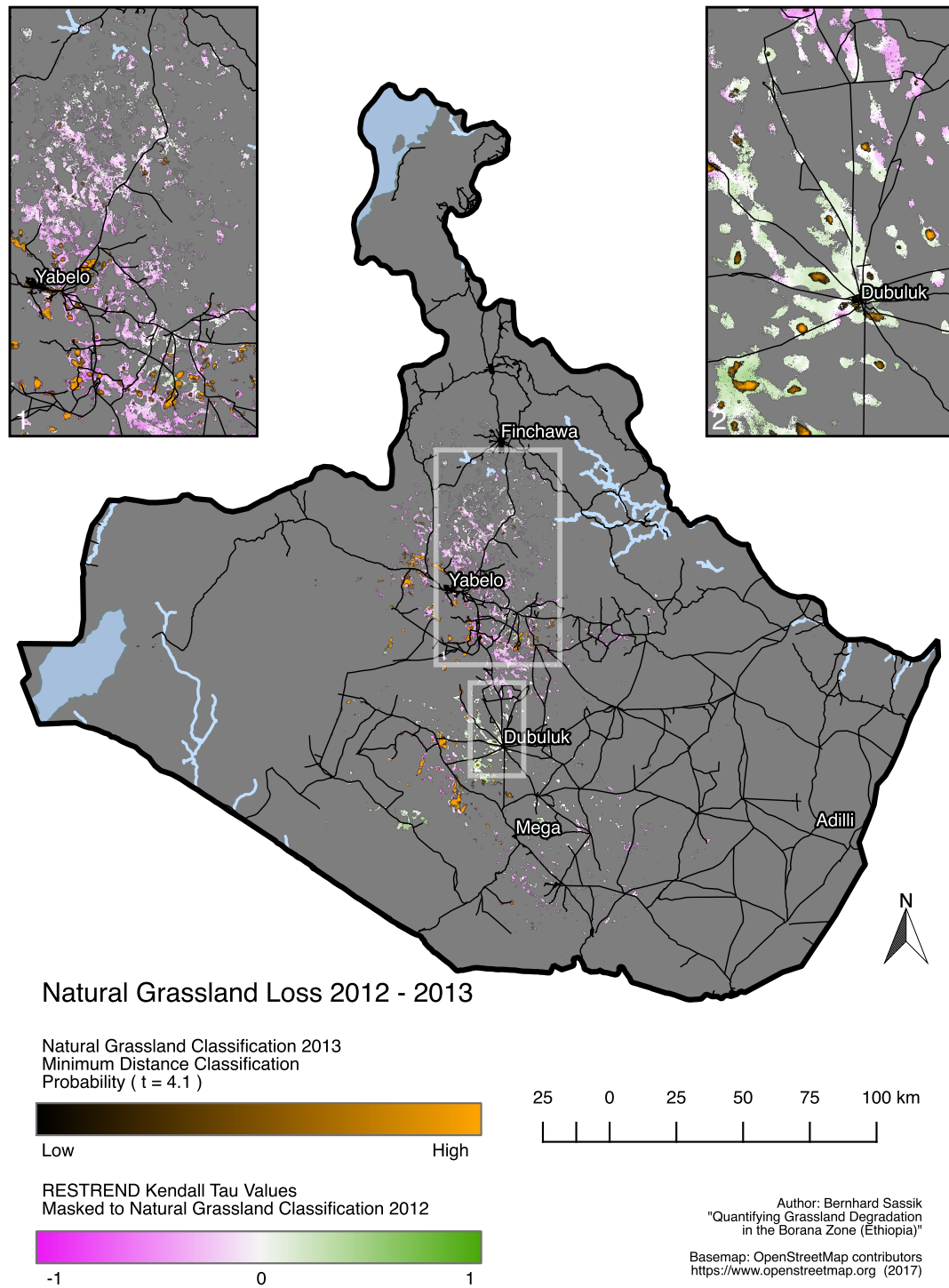


Figure 4.7: Natural Grasslands as classified in the year 2013. Results of the RESTREND Kendall tau values were masked to all pixels classified in 2012 to present areal loss. In the north, land was lost in regions with a negative Kendall's tau, while pixels of increasing photosynthetic activity dropped out in the south.

5. Discussion

2767 Landsat images of multiple scenes were processed for this study. By aggregating annual classification descriptors, problems of spatial and temporal availability constraints were tried to be overcome. Modeling data, like in this case sums of NDVI, always introduces uncertainties that need to be considered. Likewise, data availability directly influences results of data aggregations, making descriptor selections a trade-off of resolutions and approximations. The Landsat 7 Scan Line Error made spatial averaging necessary and therefore lowered the spatial resolution of respective results to some extent. Rather than providing absolute answers to questions concerning areal extents of certain classes, this study should be perceived as big data processing and aggregation work flow under very specific constraints. It provides overall tendencies, trends and relative answers. The RESTREND method is based on the basic assumption precipitation would almost linearly influence vegetation activity. Although this is per se not wrong, especially in arid parts of the world, it nevertheless is a general assumption that can be proven wrong under certain conditions. If all the rain would fall in just one day rather than in the period of a year, vegetation activity would obviously be influenced very differently. On top of all those methodological approximations and simplifications of complex processes in a long time frame, the classification itself is always only as good as its training. Even the best and most precise descriptors would not yield satisfying results, if the training is unsatisfactory. Here, ground truth information directly gathered in the field would be the gold standard. Although the developed application would certainly be capable of processing also these datasets, presented results are based on training data collected with very high resolution satellite imagery of different years and therefore are distorted.

Considering all of these problems, respective results for *Kalos*, the managed pastures around villages, and natural grasslands only show relative trends. This becomes especially apparent when setting classification distance thresholds. Different maximal distances to class centroids consequently yield other results, but basically show the same overall tendencies and trends, just on different general levels of areal extent. This threshold selection is based on personal judgments and approximations by the user under consideration of provided accuracy charts and image histograms, which further introduces uncertainties. Nevertheless, results are mapped to surface images and can be observed and interpreted visually, which is something humans can do fast and intuitively, unlike machines.

Based on the two classifications presented in the previous chapter, some general statements were extracted. They are predominantly based on logical reasoning and require further studies for certain explanations. However, these findings align with the relevant literature presented in the introduction of this thesis.

Natural grassland has higher NDVI sums than Kalos. Observing the class centroids of both classes, it is notable that they are almost identical in their shapes [Fig.4.3][Fig.4.6]. Grassland, however, has a trained NDVI sum of 9.606, while the sum for *Kalos* is 9.351. Both centroids were built without actual ground truth, but based purely on very high resolution satellite imagery, which to some extent jeopardizes the study results as a whole. But considering these values to be true, it leaves the conclusion that trained grassland shows higher vegetation activities than intensively managed pastures.

Single annual RESTREND residuals help identifying processes in a temporal context. A Kendall's tau, representing a whole RESTREND analysis, shows overall trends concerning the time series on a map. Since this single value is based on sixteen respective residuals per pixel, these individual values represent temporally high resolved partial results that enable assumptions concerning the succession of events.

Multiple reasons lead to disappearing natural grassland patches. Based on an evaluation of respective RESTREND results, it can be argued that different drivers provoke a disappearing

of grassland areas. While strongly negative trending residuals suggest land degradation in terms of conversion to bare soil [Fig.5.1], a low Kendall's tau in combination with decreasing distances to the *Kalos* centroid suggests a conversion to *Kalos*, as they have lower sums of NDVI per training definition and therefore lower photosynthetic activity. In other words, a grassland pixel showing only a damped negative Kendall's tau before dropping out of class, potentially transformed to *Kalos* [Fig.5.2]. Three reasons are suggested for disappearing patches of positive RESTREND results. Residuals of clearly ascending trend slopes identify pixels of raised photosynthetic activity. Bush encroachment is a process capable of explaining such losses under this constraint [Fig.5.3]. The rise of crop cultivation presents another possible reason, but since harvests tend to not be very successful, it is assumed that respective Kendall tau coefficients would be less pronounced [Tab.5.1]. Finally, it is possible that the increase of photosynthetic activity is not temporally correlating with respective classification distances. Around Dubuluk, grassland loss was severe while Kendall tau coefficients were high. Simultaneously, *Kalos* classification distances decreased notably. Investigative pixel inspections suggest a greening process starting in 2009 that lead to conversions from bare soil to natural grassland [Fig.5.4]. In 2012, pixels were again in transition and had temporary low distances to both class centroids. Starting in 2013, resemblance to natural grassland radically decreased, while classification distances further stayed on continuous low levels for *Kalos*. In consequence, it is assumed that these areas were transformed to managed pastures shortly after they became initially productive natural grasslands.

Kalos were gained in previous natural grassland areas and shrub lands. Gained areas in the north showed a tendency to slightly negative RESTREND taus. Since these areas were also characterized by high losses of natural grassland, a conversion to *Kalos* is suggested [Fig.5.2]. Southeast of Yabelo, pixel distances reduced drastically and symmetrically to clearly negative annual RESTREND residuals, while a previous similarity to natural grassland was not always detected. These areas lost vegetation performance and therefore became more similar to *Kalos*. Despite the ban on fire clearings of bushes and shrubs, the method is well established in the region and capable of explaining this relation [Fig.5.5]. Small areas south of Dubuluk and north of Adilli show positive residual trends in combination with decreasing classification distances. These pixels became pastures due to their greening tendencies. However, it is assumed that photosynthetic activity initially increased because former degraded land transformed to natural grassland and just in further consequence, it was occupied as *Kalos* [Fig.5.4][Tab.5.1].

Table 5.1: Grassland and pasture loss or gain was analyzed under consideration of different RESTREND results and concludes to respective assumptions concerning underlying circumstances. Fire clearing, land degradation and bush encroachment was assumed in scenarios, where a transition from natural grasslands to *Kalos* could not be detected.

Kendall Tau	-1		0	1	
Areal loss	Land degradation	Grassland becomes Kalos		Grassland becomes Agriculture	Bush encroachment
Areal gain	Fire clearing	Kalos gains Grassland			Preceding greening

5.1 Example: Land Cultivation and Degradation

The area southeast of Yabelo is characterized by natural grassland loss, partly in combination with strong negative RESTREND results. Multiple processes were revealed by pixel inspections. After 2012, distances to the natural grassland centroid increased radically while RESTREND residuals dropped. In this example, distances to *Kalos* never decreased below the threshold, which in further consequence suggests land degradation in terms of conversion to bare soil [Fig.5.1]. Before, a cyclical oscillation of classification distances is notable and indicates land management strategies like fallow periods.

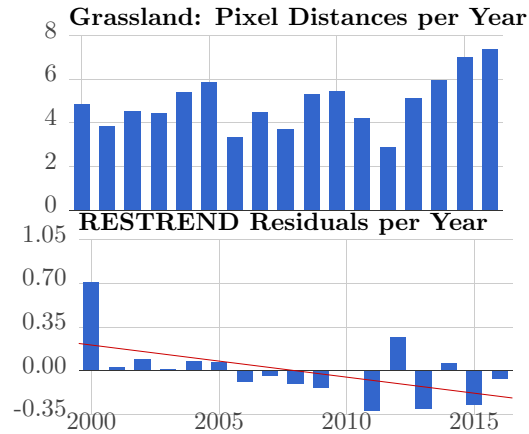


Figure 5.1: Natural grassland degradation after fallow periods: After two cycles of land cultivation and fallow, the pixel potentially degraded, since classification distances increased in correlation to negative residuals in respective years.

5.2 Example: Early Natural Grasslands to Kalos

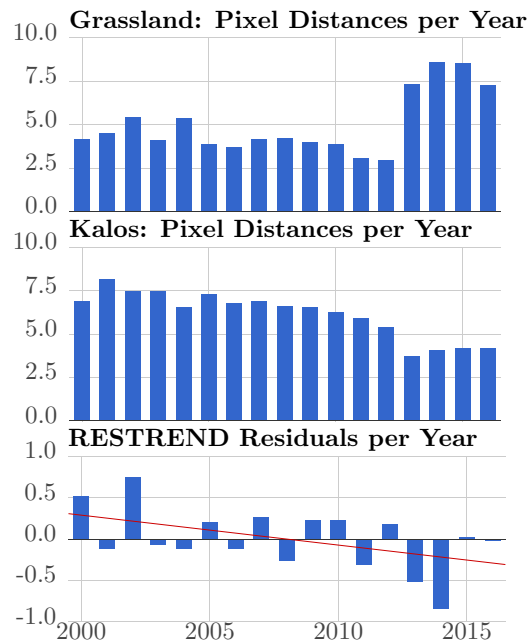


Figure 5.2: Transition from early natural grassland to managed pastures: This pixel result is symptomatic for land cover changes south of Finchawa. In years where classification distances to *Kalos* drastically dropped, residuals were particularly negative.

South of Finchawa, many pixels converted from natural grassland to *Kalos* between 2012 and 2013 [Fig.4.4][Fig.4.7]. Specifically, regions showed short distances to the natural grassland centroid since early years of the time series, before they increasingly resembled *Kalos*. For the majority, this transition is correlated to negative RESTREND residuals and also slightly negative Kendall tau coefficients well over -0.5 [Fig.5.2].

5.3 Example: Bush Encroachment

A patch of natural grassland disappeared over the period 2012 - 2013, roughly 60 km west of Mega [Fig.4.7]. These pixels had a positive Kendall's tau in common and did not transform to *Kalos*.

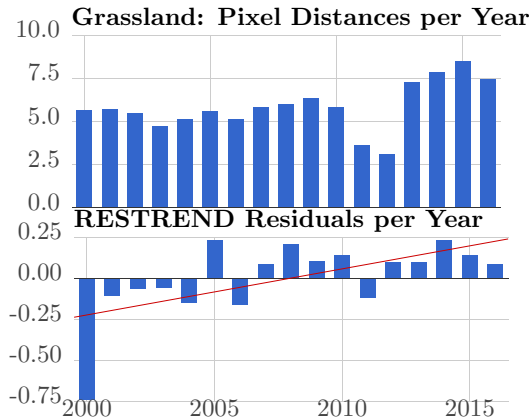


Figure 5.3: Transition from natural grassland to bushland: Good vegetation performances let classification distances sink in 2009 and therefore suggest former grassland close to degradation. When greening processes further increased, distances followed along. Bushes potentially spread as of 2013.

Their respective residuals indicate an overall greening process around 2009 which first decreased classification distances to natural grassland but further increased them again over previous levels. Corresponding charts suggest greening of degraded grassland that further resulted in bush encroachment [Fig.5.3].

5.4 Example: New Natural Grasslands to Kalos

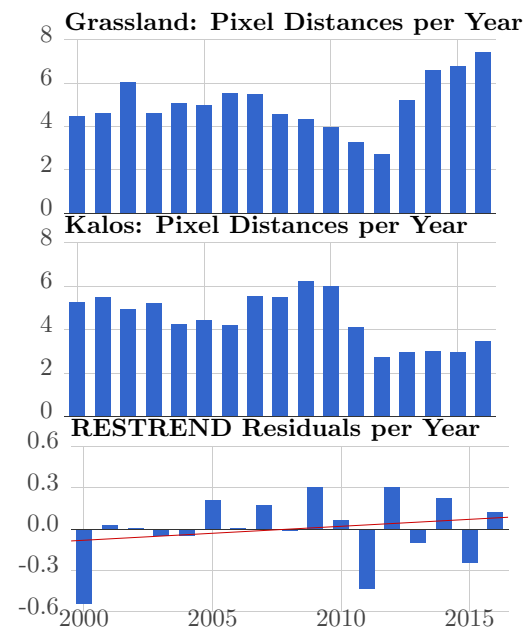


Figure 5.4: Transition from new natural grassland to managed pastures: In the area around Dubuluk, greening tendencies transformed large patches to natural grassland, but shortly after the transition, they were converted to managed pastures.

Around the settlement of Dubuluk, natural grassland was lost and *Kalos* were gained. While this transition is assumed to take place in correlation to negative Kendall tau coefficients, residuals in this area resulted in positive trends. It was concluded that greening impulses between 2007 and 2009 transformed these areas to grassland and in further consequence, between 2012 and 2013, they were re-functioned as *Kalos* [Fig.5.4].

5.5 Example: Fire Clearing

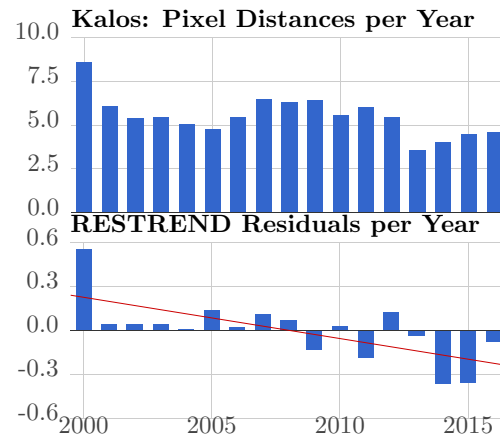


Figure 5.5: Fire clearing: With a severe drop of residuals, the pixel in this example became more similar to the *Kalos* class centroid.

Newly gained *Kalos* patches with a negative Kendall's tau and former low resemblance to natural grassland, indicate fire clearings. These pixels became more similar to managed pastures due to their rather radical loss of vegetation activity.

6. Conclusion

The results show a clear accumulation of grassland pixels, natural and managed, in the central regions of the Borana Zone. Locations of settlements and villages are linked to the presence of such grasslands, likewise, spatial distribution in large scales gives the impression of the influence of former water bodies, although this was not further investigated. *Kalos* became an increasingly present land cover type starting in 2010 and spread especially over previous former grasslands. This is just one of the reasons for disappearing grassland patches in the Borana Zone. Bush encroachment and land degradation to bare soil are other factors responsible for a radically shrinking grassland extent as of 2013. All of these are reported and known dynamics in the region, although other relevant studies did not consider the concatenation of these different processes in a broader time frame. Generally, a north-south difference can be observed in such, that grassland was lost in the north predominantly due to losses in vegetation activity, while good photosynthetic performances converted degraded grasslands to managed pastures in the south. This happened in correlation to general spatial and temporal patterns of precipitation [Fig2.1][Fig.2.2].

Future developments will be highly dependent on these precipitation patterns and anomalies like droughts or flipped rain seasons, but in general it is assumed that *Kalos* land cover shares will further increase due to active transformation efforts by regional pastoralists. This dynamic will consequently raise pressure on natural grasslands, which already suffer from degradation processes and bush encroachment. The results suggest a new equilibrium for natural grassland areal extents, that is roughly half the pre-2010 level. However, a reintroduction of fire clearing in selected patches west of Mega would very likely allow natural pastures to regrow, since the grassland loss in these areas is not connected to degradation tendencies. Despite countermeasures like fallow periods, the central region south of Yabelo largely suffered from degradation processes starting in 2013. Overexploitation needs to be prevented and land management strategies will further gain importance in order to minimize damages, but future rainfalls will dictate the final result of this region's transformation process.

References

- [1] T. Abate and A. Angassa. Conversion of savanna rangelands to bush dominated landscape in Borana, Southern Ethiopia. *Ecological Processes*, 5(1):6, 2016. doi:10.1186/s13717-016-0049-1.
- [2] I. Ali, F. Cawkwell, E. Dwyer, B. Barrett, and S. Green. Satellite remote sensing of grasslands: from observation to management. *Journal of Plant Ecology*, 9(6):649–671, 2016. doi:10.1093/jpe/rtw005.
- [3] A. Angassa. Effects of drought on cattle herd dynamics and its implication on local livelihood systems in Borana , Ethiopia. *FSC Brief No. 1, University of Hohenheim, Germany*, (1):1–6, 2011.
- [4] A. Angassa and G. Oba. Herder perceptions on impacts of range enclosures, crop farming, fire ban and bush encroachment on the rangelands of Borana, Southern Ethiopia. *Human Ecology*, 36(2):201–215, 2008. doi:10.1007/s10745-007-9156-z.
- [5] E. Assefa and B. Hans-Rudolf. Farmers’ perception of land degradation and traditional knowledge in Southern Ethiopia - resilience and stability. *Land Degradation & Development*, 27(6):1552–1561, 2016. doi:10.1002/ldr.2364.
- [6] R. De Jong and S. De Bruin. Linear trends in seasonal vegetation time series and the modifiable temporal unit problem. *Biogeosciences*, 9(1):71–77, 2012. doi:10.5194/bg-9-71-2012.
- [7] R. de Jong, S. de Bruin, A. de Wit, M. E. Schaepman, and D. L. Dent. Analysis of monotonic greening and browning trends from global NDVI time-series. *Remote Sensing of Environment*, 115(2):692–702, 2011. doi:10.1016/j.rse.2010.10.011.
- [8] S. Foga, P. L. Scaramuzza, S. Guo, Z. Zhu, R. D. Dilley, T. Beckmann, G. L. Schmidt, J. L. Dwyer, M. Joseph Hughes, and B. Laue. Cloud detection algorithm comparison and validation for operational Landsat data products. *Remote Sensing of Environment*, 194:379–390, 2017. doi:10.1016/j.rse.2017.03.026.
- [9] N. Gorelick, M. Hancher, M. Dixon, S. Ilyushchenko, D. Thau, and R. Moore. Google Earth Engine: Planetary-scale geospatial analysis for everyone, 2016. doi:10.1016/j.rse.2017.06.031.
- [10] G. ([https://stats.stackexchange.com/users/805/glen b](https://stats.stackexchange.com/users/805/glen_b)). How to find a good fit for semi-sinusoidal model in R?, 2013. URL: <https://stats.stackexchange.com/q/60504>.
- [11] G. J. Huffman. 3B42 Version 7 Web Description, 2013. URL: <https://trmm.gsfc.nasa.gov/3b42.html>.
- [12] G. J. Huffman. The Transition in Multi-Satellite Products from TRMM to GPM (TMPA to IMERG), 2015. URL: <https://pmm.nasa.gov/resources/documents/transition-multi-satellite-products-trmm-gpm-tpa-imerg>.
- [13] G. J. Huffman, D. T. Bolvin, E. J. Nelkin, D. B. Wolff, R. F. Adler, G. Gu, Y. Hong, K. P. Bowman, and E. F. Stocker. The TRMM Multisatellite Precipitation Analysis (TMPA): Quasi-Global, Multiyear, Combined-Sensor Precipitation Estimates at Fine Scales. *Journal of Hydrometeorology*, 8(1):38–55, 2007. doi:10.1175/JHM560.1.
- [14] B. Mack, R. Roscher, and B. Waske. Can i trust my one-class classification? *Remote Sensing*, 6(9):8779–8802, 2014. doi:10.3390/rs6098779.

-
- [15] B. L. Markham, J. C. Storey, D. L. Williams, and J. R. Irons. Landsat sensor performance: history and current status. *IEEE Transactions on Geoscience and Remote Sensing*, 42(12):2691–2694, 2004. doi:10.1109/TGRS.2004.840720.
- [16] B. K. Michael Elias, Oliver Hensel, Uwe Richter, Christian Hülsebusch and O. Wasonga. Land Conversion Dynamics in the Borana Rangelands of Southern Ethiopia: An Integrated Assessment Using Remote Sensing Techniques and Field Survey Data. *Environments*, 2:1–31, 2015. doi:10.3390/environments2010001.
- [17] T. B. Solomon, H. A. Snyman, and G. N. Smit. Cattle-rangeland management practices and perceptions of pastoralists towards rangeland degradation in the Borana zone of southern Ethiopia. *Journal of Environmental Management*, 82(4):481–494, 2007. doi:10.1016/j.jenvman.2006.01.008.
- [18] B. Tache and G. Oba. Is Poverty Driving Borana Herders in Southern Ethiopia to Crop Cultivation? *Human Ecology*, 38(5):639–649, 2010. doi:10.1007/s10745-010-9349-8.
- [19] USAIDAfrica. Climate Change & The Negelle Accords, 2014. URL: <https://www.youtube.com/watch?v=9MFPyi6jxR0>.
- [20] K. J. Wessels, F. V. D. Bergh, R. J. Scholes, F. van den Bergh, and R. J. Scholes. Limits to detectability of land degradation by trend analysis of vegetation index data. *Remote Sensing of Environment*, 125:10–22, 2012. doi:10.1016/j.rse.2012.06.022.

Appendix

For registered Google Earth Engine users, the developed application is available at <https://code.earthengine.google.com/ec6c0ca785edabc18e8b2dc64a43b18d> .

Please note that some complex results were preprocessed and imported for a faster computational performance (indicated in the import section at the top). Therefore, the app can not simply be used in another region of interest.

Declaration

Personal declaration: I hereby declare that the submitted thesis is the result of my own, independent work. All external sources are explicitly acknowledged in the thesis.